# Analyst

## PAPER

Check for updates

Cite this: DOI: 10.1039/c8an00138c

# Metal ions induced secondary structure rearrangements: mechanically interlocked lasso vs. unthreaded branched-cyclic topoisomers†

Kevin Jeanne Dit Fouque,[a] Javier Moreno,[a] Julian D. Hegemann,[b] Séverine Zirah, [c] Sylvie Rebuffat[c] and Francisco Fernandez-Lima [*a]

Metal ions can play a significant role in a variety of important functions in protein systems including co-factor for catalysis, protein folding, assembly, structural stability and conformational change. In the present work, we examined the influence of alkali (Na, K and Cs), alkaline earth (Mg and Ca) and transition (Co, Ni and Zn) metal ions on the conformational space and analytical separation of mechanically interlocked lasso peptides. Syanodin I, sphingonodin I, caulonodin III and microcin J25, selected as models of lasso peptides, and their respective branched-cyclic topoisomers were submitted to native nESI trapped ion mobility spectrometry-mass spectrometry (TIMS-MS). The high mobility resolving power of TIMS permitted to group conformational families regardless of the metal ion. The lower diversity of conformational families for syanodin I as compared to the other lasso peptides supports that syanodin I probably forms tighter binding interactions with metal ions limiting their conformational space in the gas-phase. Conversely, the higher diversity of conformational families for the branched-cyclic topologies further supports that the metal ions probably interact with a higher number of electronegative groups arising from the fully unconstraint C-terminal part. A correlation between the lengths of the loop and the C-terminal tail with the conformational space of lasso peptides becomes apparent upon addition of metal ions. It was shown that the threaded C-terminal region in lasso peptides allows only for distinct interactions of the metal ion with either residues in the loop or tail region. This limits the size of the inter-acting region and apparently leads to a bias of metal ion binding in either the loop or tail region, depend-ing whichever section is larger in the respective lasso peptide. For branched-cyclic peptides, the non-restricted C-terminal tail allows metal coordination by residues throughout this region, which can result in gas-phase structures that are sometimes even more compact than the lasso peptides. The high TIMS resolution also resulted in the separation of almost all lasso and branched-cyclic topoisomer metal ions ($r \sim 2.1$ on average). It is also shown that the metal incorporation (e.g., doubly cesiated species) can lead to the formation of a simplified IMS pattern (or preferential conformers), which results in baseline analyti-cal separation and discrimination between lasso and branched-cyclic topologies using TIMS-MS.

[a]Department of Chemistry and Biochemistry, Florida International University, Miami, FL 33199, USA. E-mail: fernandf@fiu.edu
[b]Department of Chemistry, University of Illinois, Urbana-Champaign, IL 61801, USA
[c]Laboratory Molecules of Communication and Adaptation of Microorganisms, National Museum of Natural History, Sorbonne Univ, 75005 Paris, France
†Electronic supplementary information (ESI) available: 3D representation of class II lasso peptides, scheme of the TIMS cell, correlation of the $\overline{CCS}$ of the doubly protonated species of lasso and branched-cyclic peptides as a function of the molecular mass, effect of the metalated species on the lasso conformational spaces as a function of the loop size, TIMS spectra of the investigated lasso peptides and their branched-cyclic topoisomers cationized by alkali, alkaline earth and transition metalated species, conditions for the production of lasso peptides, and tables of the measured CCS and resolution for all lasso and branched-cyclic ions. See DOI: 10.1039/c8an00138c

Metal ions play a vital role in many biological processes.[1] They act in a variety of important functions in protein systems including enzyme catalysis, protein folding, assembly, structural stability and conformational change.[2,3] The presence or absence of a specific metal ion is crucial to the conformational space and/or chemical functionality of over one third of all proteins.[1,4] Several structural studies aimed to determine the binding site locations,[5–7] the nature of metal ion coordination,[8–10] and the role of metal–ligand interactions on structure and function.[11,12] Interactions between metal ions and biomolecules have been investigated using well established techniques such as circular dichroism,[13,14] nuclear magnetic resonance (NMR) spectroscopy,[15,16] and X-ray crystallography.[17,18] Furthermore, the structures of metal-containing

peptides and proteins in the gas-phase have been reported using mass spectrometry[19–23] equipped with soft ionization sources such as electrospray ionization (ESI).[24] Interestingly, the addition of metal ions often influences the fragmentation patterns upon activation.[25–28] In addition, the potential of metal ions to differentiate isomer species, which present the same fragmentation pattern, has been shown using tandem mass spectrometry.[29–33] All these results suggest the existence of highly-specific metal-binding sites.

The interaction of peptides and proteins with metal ions has been a subject of considerable interest in ion mobility spectrometry coupled to mass spectrometry (IMS-MS) since the pioneering work of Clemmer and Jarrold.[34–42] These studies showed the potential of IMS-MS to provide a more detailed understanding of the basic interactions that occur and represent an important step in the conformational engineering of peptides and proteins. In addition, the implementation of the IMS technique makes the use of metal ions a powerful tool for the separation of isomers which are present in close conformational spaces. In fact, metalated biomolecules in the gas phase tend to differ in conformation from their protonated analogs, as the metal ion can be multiply charged, can bind to single/multiple sites, and/or coordinates differently because of specific chemistry.[43] If these deviations are unequal for two isomer species, metalation can potentially enhance their separation in IMS devices with modest resolving power ($R \sim 30$–60).[44–47] The push for higher resolution and sensitivity has led to the development of other forms of IMS devices, including trapped IMS (TIMS).[48,49] The coupling of TIMS-MS[48–53] has found multiple applications in analytical workflows which need high mobility resolving power ($R$ up to $\sim 400$).[54] TIMS-MS devices have proven useful for rapid separation and structural elucidation of biomolecules,[53,55–65] for screening[55] and targeted[51,53] analysis of complex mixtures, tracking isomerization kinetics,[56–58] characterizing the conformational spaces of peptides,[66] separation of D-amino acid containing peptides,[67] DNA,[59] proteins,[68,69] and macromolecular complexes in native and denatured states.[70] The effect of metal incorporation in peptide systems has not been reported using TIMS devices, although similar analytical enhancement to those observed previously with other variants of IMS are expected.

Research on metal–peptide systems provides a basis for understanding metal interactions occurring in biochemically relevant systems. In particular, class II lasso peptides are a structurally fascinating class of ribosomally synthesized and post-translationally modified peptides (RiPPs) exhibiting a unique mechanically interlocked topology.[71,72] They display a rigid and compact structure where the C-terminal tail is threaded through and trapped within an N-terminal macrolactam ring, leading to a [1]rotaxane type structure (Fig. S1†). Strong sterical constraints, which come from bulky amino acids located above and below the macrolactam ring that are called plugs, stabilize the entropically disfavored lasso structure. Many lasso peptides were discovered through genome mining approaches and isolation and characterization of new

representatives of this RiPP family is still an active area of research.[73–78] Diverse biological activities have been reported for class II lasso peptides, including antimicrobial, enzyme inhibitory or receptor antagonistic properties.[71,72] The extraordinary rigid and compact structure of the mechanically interlocked lasso topologies, together with their panel of biological activities makes them a promising scaffold for next generation drug design.[79,80] One limitation to the activity and further developments of lasso peptides is the unthreading of the C-terminal tail, a trend reported for certain lasso peptides, which yield their corresponding branched-cyclic topoisomers, although there are also numerous examples of lasso peptides that are resistant to thermally-induced unthreading.[73,81–83]

In this study, four mechanically interlocked lasso peptides, caulonodin III, microcin J25, sphingonodin I and syanodin I, with their corresponding unthreaded branched-cyclic topoisomers were investigated using native nESI-TIMS-MS (Table 1). These four lasso peptides were specifically selected according to the lengths of the loop and the C-terminal tail region which could provide different binding interactions with the metal ions. In the following discussion, a special emphasis will be placed on the influence of alkali (Na, K and Cs), alkaline earth (Mg and Ca) and transition (Co, Ni and Zn) metal ions on lasso and branched-cyclic topoisomer ion conformation and separation.

# Experimental section

## Materials and reagents

Microcin J25 was produced, as described previously,[84] by cultivation of *Escherichia coli* MC4100 harboring the plasmid pTUC202,[85] in M63 medium at 37 °C for 16 h. Caulonodin III,[73] sphingonodin I,[73] and syanodin I[73] were produced heterologously in *E. coli* BL21 (DE3), as described elsewhere (Table S1†). Briefly, the purification procedures were started with centrifugation to separate cell pellets and culture supernatants. Microcin J25 was extracted from the culture supernatants by solid phase extraction using SepPak $C_8$ or $C_{18}$ reversed-phase cartridges (Waters). The elution was performed using water with 0.1% formic acid and acetonitrile mixtures with increasing content of acetonitrile, and the fractions of interest were then evaporated under reduced pressure. A second purification step was performed by reversed-phase high performance liquid chromatography (HPLC). Caulonodin III, sphingonodin I and syanodin I were isolated from cell pellets by extraction with methanol. The resulting extracts were directly subjected to HPLC purification steps as described previously.

The branched-cyclic peptide of syanodin I was obtained by heating the lasso peptide at 95 °C for 3 h and was subsequently purified by reversed-phase HPLC. For caulonodin III, microcin J25 and sphingonodin I, which are heat stable lasso peptides, topoisomeric variants were obtained by solid-phase synthesis from Genepep (St Jean de Védas, France). The

**Table 1** Summary of the studied lasso and branched-cyclic peptides. The macrolactam rings are highlighted in green, the loops in blue, the plugs in red and the C-terminal tails in orange. The proposed plugs-of lasso peptides, for which the 3D structures have not been determined, are colored in purple

| Peptide | Sequence | Molecular mass (Da) | Topology |
|---|---|---|---|
| Syanodin I | GISGGTVD$_8$APAGQGLAG$_{16}$ | 1409.50 | |
| Syanodin I branched-cyclic | GISGGTVD$_8$APAGQGLAG$_{16}$ | 1409.50 | |
| Sphingonodin I | GPGGITGD$_8$VGLGENNFG$_{17}$ | 1542.61 | |
| Sphingonodin I branched-cyclic | GPGGITGD$_8$VGLGENNFG$_{17}$ | 1542.61 | |
| Caulonodin III | GQIYDHPE$_8$VGIGAYGCE$_{17}$ | 1789.92 | |
| Caulonodin III branched-cyclic | GQIYDHPE$_8$VGIGAYGCE$_{17}$ | 1789.92 | |
| Microcin J25 | GGAGHVPE$_8$YFVGIGTPISFYG$_{21}$ | 2107.32 | |
| Microcin J25 branched-cyclic | GGAGHVPE$_8$YFVGIGTPISFYG$_{21}$ | 2107.32 | |

carbonate salts of Na, K, Cs, Mg, Ca, Co, Ni and Zn were purchased from Acros Organics (New Jersey, USA). The peptides were dissolved in 10 mM NH$_4$Ac (native conditions) to 5 µM with or without 70 µM of a carbonate salt. The instrument was initially calibrated using the Tuning Mix[50] from Agilent (Santa Clara, CA).

**TIMS-MS experiments**

We employed a custom nESI-TIMS unit coupled to an Impact Q-TOF mass spectrometer (Bruker, Billerica, MA).[48,49] The TIMS unit is run by custom software in LabView (National Instruments) synchronized with the MS platform controls.[49] Sample aliquots (10 µL) were loaded in a pulled-tip capillary biased at 700–1200 V to the MS inlet. TIMS separation depends on the gas flow velocity ($v_g$), elution voltage ($V_{elution}$),

ramp time ($t_{ramp}$) and base voltage ($V_{out}$).[48,86] The mobility, $K$, is defined by:

$$K = \frac{v_g}{E} \cong \frac{A}{(V_{elution} - V_{out})} \qquad (1)$$

The mobility calibration was determined using known reduced mobilities of Tuning Mix components ($K_0$ of 1.013, 0.835, and 0.740 cm$^2$ (V s)$^{-1}$ for respective $m/z$ 622, 922, and 1222) using the method previously described.[50] The buffer gas was N$_2$ at ambient temperature ($T$) with $v_g$ set by the pressure difference between the funnel entrance ($P1$ = 2.6 mbar) and exit ($P2$ = 1.1 mbar, Fig. S2†). An rf voltage of 200$V_{pp}$ at 880 kHz was applied to all electrodes. A typical scan rate (Sr = $\Delta V_{ramp}/t_{ramp}$) of 0.56 V m$^{-1}$ s$^{-1}$ was used. The measured mobi-

lities were converted into CCS (Å$^2$) using the Mason–Schamp equation:

$$\Omega = \frac{(18\pi)^{1/2}}{16}\frac{q}{(k_\mathrm{B}T)^{1/2}}\left(\frac{1}{m}+\frac{1}{M}\right)^{1/2}\frac{1}{N}\times\frac{1}{K} \qquad (2)$$

where $q$ is the ion charge, $k_\mathrm{B}$ is the Boltzmann constant, $N$ is the gas number density, $m$ is the ion mass, and $M$ is the gas molecule mass.[86] The IMS peaks were fitted with Gaussian distributions using OriginPro 2016. The resolution $r$ is defined as $r = 1.18 \times (\Omega_2 - \Omega_1)/(w_1 + w_2)$, where $w$ is the full peak width at half maximum (FWHM).

# Results and discussion

## Influence of metal ions on lasso and branched-cyclic topoisomer ion conformation

The distribution of lasso and branched-cyclic peptide ions (either protonated, or containing metal ions) mostly displayed [M + 2H]$^{2+}$, [M + H + X]$^{2+}$ and/or [M + 2X]$^{2+}$ charge state species when using native nESI. Typical high resolution TIMS spectra for protonated and metalated forms of the individual lasso peptides (caulonodin III, microcin J25, sphingonodin I and syanodin I) and their corresponding unthreaded branched-cyclic topoisomers are shown in Fig. 1 and S3† and their collision cross sections (CCS) are listed in Tables S2–S5.†
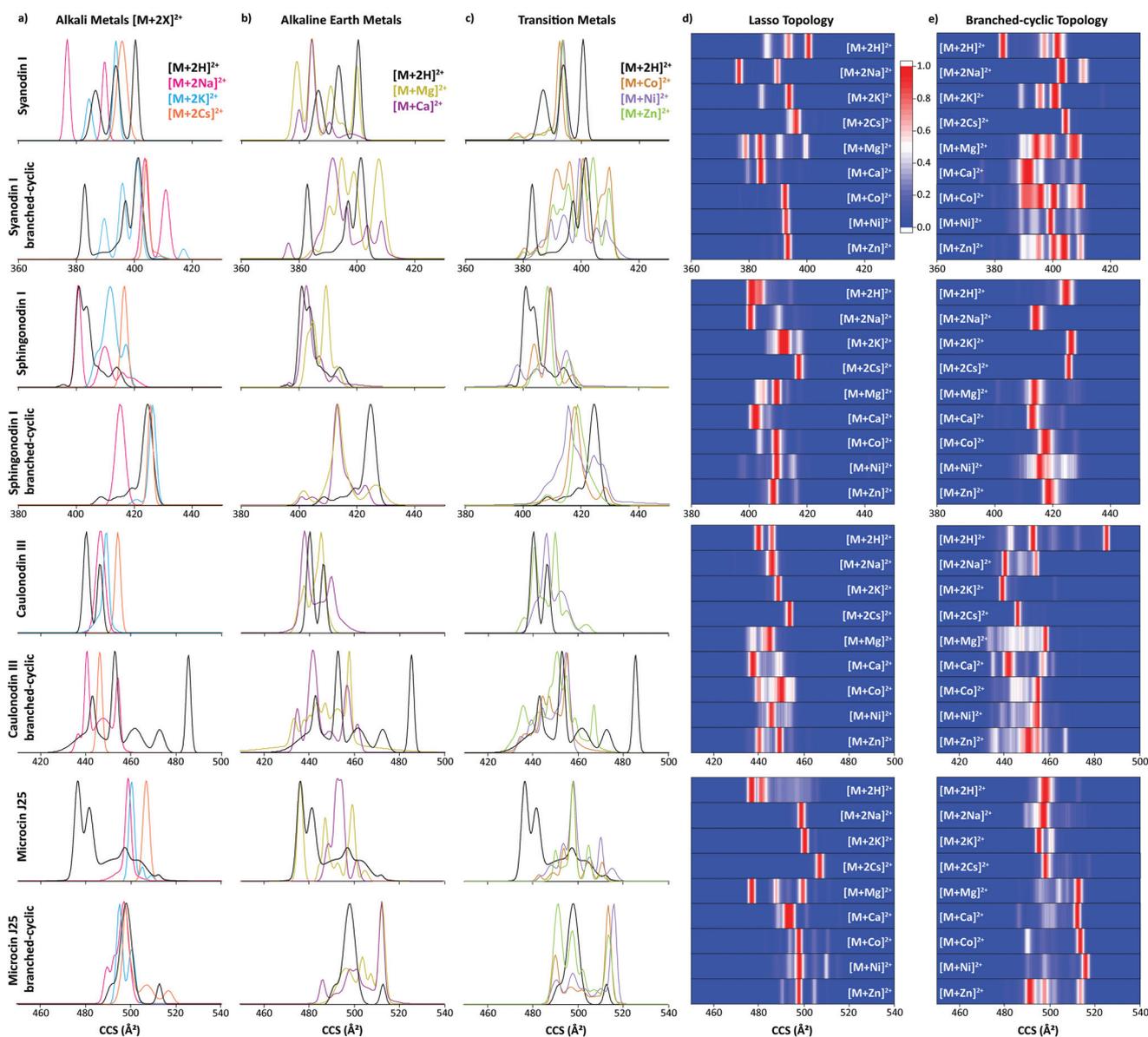


Fig. 1 Typical TIMS spectra of lasso and branched-cyclic topoisomers of the protonated (black), sodiated (magenta), potassiated (light blue), cesiated (dark orange), magnesiated (yellow), calciated (purple), cobaltiated (brown), nickelated (light purple) and zincated (light green) species. Corresponding heat maps are shown in (d) and (e). A typical Sr of 0.56 V m$^{-1}$ s$^{-1}$ was used.

As previously reported,[87] the high resolution of TIMS permitted the separation of multiple IMS bands for the protonated lasso and branched-cyclic peptides (highlighted in black in Fig. 1). The observation of multiple compact and extended conformations suggested the presence of several combinations of intramolecular charge-driven and/or hydrogen bond interactions, especially between residues in the flexible C-terminal tail (highlighted in orange in Table 1) and the macrolactam ring (in green).[88–90] It is difficult to predict the charge localization as well as the effect of substituting protons for metal ions on the conformational space. In fact, a previous work has shown that replacing a proton by a sodium in polyalanine chains reduces the abundance of globular structures by promoting more extended conformations,[91] while another study reported a decrease in CCS leading to more compact structures.[37] These results provide evidence that sodium ions interact in different ways with functional groups of the peptide backbone and thereby are stabilizing the gas-phase conformation. We predict that the multiple interactions between the metal ions and the peptides under a given conformation will probably be stabilized through the electronegative groups.

Although solution conditions were designed to favor metalated peptide ions, protonated species were also observed. All of the metalated species studied here led to noticeable changes in the CCS distributions as compared to the protonated species (Fig. 1 and S3†). CCS values generally increased upon incorporating metal ions for lasso peptides except for syanodin I. For example, the doubly cesiated species (highlighted in dark orange in Fig. 1a) of sphingonodin I, caulonodin III and microcin J25 led to a relative mobility increase of 4.0%, 3.2% and 6.5%, respectively. Conversely, the relative CCS appears to be smaller when replacing a proton by metal ions in syanodin I (Fig. 1 and S3†). For example, the doubly cesiated species (highlighted in dark orange in Fig. 1a) led to a relative mobility decrease of 1.5%. This suggests that syanodin I probably forms tighter binding interactions with these metals than sphingonodin I, caulonodin III and microcin J25. In the case of the branched-cyclic peptides, the shifts of the metalated compared to protonated species are generally less pronounced than for the lasso peptides (Fig. 1). This suggests that the metal ions probably bind with a higher number of electronegative groups than the lasso peptides. In fact, metal ions can more easily interact with the full flexible C-terminal part of the unconstraint branched-cyclic peptides than the mechanically interlocked topology (Fig. 1).

Comparison of the TIMS profiles of the metalated species showed common bands regardless of the metal ion incorporated (Fig. 1d, e and S3 and Tables S2–S5†). For example, IMS profiles for syanodin I can be grouped in at least four conformational families (Fig. 1d and S3 and Table S2†). The IMS band at ~377 $\text{Å}^2$ is observed by adding one or two sodium, a magnesium and a calcium. The IMS band at ~387 $\text{Å}^2$ is observed in the protonated, cesiated, doubly sodiated, magnesiated and calciated species. The IMS band at ~394 $\text{Å}^2$ is common to all the metal ions except with two sodium and a calcium. The motif at ~401 $\text{Å}^2$ is preserved for the protonated, singly alkali and alkaline earth metalated ions.

In the case of sphingonodin I, the IMS profiles can be grouped in at least six conformational families (Fig. 1d and S3 and Table S3†). The IMS band at ~396 $\text{Å}^2$ is observed with the protonated, calciated and nickelated species. The IMS band at ~401 $\text{Å}^2$ is observed with the protonated species and by adding two sodium, a magnesium, a calcium and a zinc. The IMS band at ~404 $\text{Å}^2$ is observed for the protonated and all the metalated species except for the doubly sodiated and cesiated species. The IMS band at ~410 $\text{Å}^2$ is observed for the transition metal ions, magnesium and all the alkali metal ions except in the case of the doubly cesiated species. The IMS band at ~415 $\text{Å}^2$ is common to all the investigated metal ions, while the IMS band at ~420 $\text{Å}^2$ is observed for all singly alkali and doubly sodiated species.

In the case of caulonodin III, the IMS profiles can be grouped in at least five conformational families (Fig. 1d and S3 and Table S4†). The IMS band at ~436 $\text{Å}^2$ is observed with the alkaline earth and zincated species. The IMS band at ~440 $\text{Å}^2$ is observed with the protonated species and by adding alkaline earth and transition metal ions. The IMS band at ~446 $\text{Å}^2$ is common to all the metal ions except for the cesiated species. The IMS band at ~449 $\text{Å}^2$ is preserved for one cesium, two potassium and for all alkaline earth and transition metal ions. The IMS band at ~454 $\text{Å}^2$ is observed only for the doubly cesiated, cobaltiated and zincated species.

In the case of microcin J25, the IMS profiles can be grouped in at least six conformational families (Fig. 1d and S3 and Table S5†). The IMS band at ~476 $\text{Å}^2$ is observed with the protonated, singly sodiated and potassiated and magnesiated species. The IMS band at ~482 $\text{Å}^2$ is observed with the protonated species and by adding one sodium, a magnesium, a cobalt and a nickel. The IMS band at ~490 $\text{Å}^2$ is observed for the protonated and all the metalated species except for the doubly alkali and singly cesiated species. The IMS band at ~496 $\text{Å}^2$ is observed for the protonated, doubly sodiated and potassiated and all the alkaline earth and transition metalated ions. The IMS band at ~505 $\text{Å}^2$ is common to all the investigated metal ions except for the sodiated and singly potassiated species. The IMS band at ~510 $\text{Å}^2$ is observed for the protonated, singly cesiated, doubly potassiated and all the transitions metalated species.

In the case of the branched-cyclic form of syanodin I, at least nine conformational families are observed for all the investigated metal ions (Fig. 1e and S3 and Table S2†). The IMS band at ~379 $\text{Å}^2$ is observed with the calciated, cobaltiated and zincated species. The IMS band at ~385 $\text{Å}^2$ is observed with the protonated species and by adding one potassium, one cesium and all the alkaline earth and transition metal ions. The IMS band at ~390 $\text{Å}^2$ is observed for the protonated, doubly potassiated, alkaline earth and transition metalated species. The IMS band at ~394 $\text{Å}^2$ is observed for the protonated and by incorporating one potassium, a magnesium, a nickel and a zinc metal ion. The IMS band at ~397 $\text{Å}^2$ is common to all the investigated metal ions except for the singly

cesiated, doubly sodiated and nickelated species. The IMS band at ~401 Å² is observed for all the metal ions except for the doubly sodiated and cesiated and alkaline earth metalated species. The IMS band at ~405 Å² is observed for all the metal ions except for the protonated, potassiated, singly cesiated and magnesiated species. The IMS band at ~409 Å² is common to all the studied metal ions except for the protonated and the singly sodiated and cesiated species. The IMS band at ~417 Å² is only observed by adding two potassium.

In the case of the branched-cyclic form of sphingonodin I, the IMS profiles of all the metal ions studied can be divided in at least six conformational families (Fig. 1e and S3 and Table S3†). The IMS band at ~404 Å² is observed by incorporating one sodium, a magnesium and a calcium metal ion. The IMS band at ~408 Å² is observed for the protonated, singly potassiated and all the transition metalated species. The IMS band at ~415 Å² is observed with the protonated species and by adding two sodium, a magnesium, a calcium and a nickel metal ion. The IMS band at ~419 Å² is common to the protonated, singly sodiated, doubly potassiated and all the transition metalated species. The IMS band at ~425 Å² is observed for all the metal ions except for the sodiated, magnesiated, cobaltiated and zincated species. The IMS band at ~429 Å² is common for the singly alkali, magnesiated, cobaltiated and nickelated species.

In the case of caulonodin III branched-cyclic, the IMS profiles can be grouped in at least nine conformational families (Fig. 1e and S3 and Table S4†). The IMS band at ~433 Å² is only observed by incorporating a sodium metal ion. The IMS band at ~438 Å² is observed for all the metal ions except for the singly potassiated and cesiated species. The IMS band at ~443 Å² is common to all the studied metalated species. The IMS band at ~448 Å² is observed by adding one cesium, two sodium, a magnesium, a calcium, a cobalt and a zinc metal ion. The IMS band at ~454 Å² is observed for all metal ions except for the cesiated and doubly potassiated species. The IMS band at ~460 Å² is observed for all the metal ions except for the doubly sodiated and cesiated, cobaltiated and nickelated species. The IMS band at ~472 Å² is observed for the protonated, singly potassiated and cesiated and zincated species. The IMS bands at ~480 and ~485 Å² are characteristic of the insertion of one potassium and without metal ion, respectively.

In the case of the branched-cyclic form of microcin J25, the IMS profiles of all the metal ions studied can be divided in at least seven conformational families (Fig. 1e and S3 and Table S5†). The IMS band at ~477 Å² is observed by incorporating a single sodium, potassium and cesium metal ion. The IMS band at ~487 Å² is observed only for the sodiated and calciated species. The IMS band at ~491 Å² is observed with all the metal ions except for the singly sodiated, doubly cesiated and magnesiated species. The IMS band at ~498 Å² is common to all the investigated metalated species. The IMS band at ~505 Å² is observed for the singly sodiated and potassiated, doubly cesiated, magnesiated and all the transition metalated species. The IMS band at ~513 Å² is common in the protonated species and by incorporating all the alkaline earth and transition metal ions. The conformation at ~517 Å² is only observed by adding two cesium and a nickel metal ion.

The lower number of conformational families for syanodin I as compared to the other lasso peptides suggests that syanodin I forms tighter binding interactions with all the studied metal ions limiting their conformational changes in the gas-phase. Conversely, the higher number of conformational families for the branched-cyclic topologies further supports that the metal ions probably interact with a higher number of electronegative groups arising from the unconstraint C-terminal part as compared to the mechanically interlocked lasso structures.

Comparison of CCS for species with similar masses provides some insight about the conformational range of different isomeric structures that are present in the gas-phase. For lasso peptides, due to larger structural constraints in their secondary structure, it is expected that the interaction with the metal ion will have a lower effect than for the branched-cyclic peptides. That is, secondary structure elements of the mechanically interlocked lasso topologies may be preserved or stabilized upon metal ion binding while more changes are expected for the branched-cyclic topologies due to the unthreaded flexible C-terminal part. The relatively complex TIMS distribution (*i.e.*, existence of multiple bands) makes it challenging to estimate the influence of metalated species on the conformational spaces of the lasso and branched-cyclic topologies. Therefore, determination of the weighted average CCS ($\sum$(CCS × intensity)/($\sum$intensity), based on the CCS reported in Tables S2–S5†) in order to get a unique $\overline{CCS}$ value for every doubly charged species proved to be a better approach. At first, we plotted the $\overline{CCS}$ values as a function of the molecular mass for all the investigated species as a way to assess the conformational trend (Fig. 2a). A strong correlation of increasing $\overline{CCS}$ with the molecular mass was obtained for syanodin I, sphingonodin I, caulonodin III and microcin J25 with their corresponding branched-cyclic topoisomers (Fig. 2a). In addition, the two correlations shown in Fig. S4a† revealed that the branched-cyclic structures are more extended than the lasso ones regardless of the molecular mass.

Comparison between the $\overline{CCS}_H$ and the $\overline{CCS}_{Metal}$ enables to efficiently illustrate the metalation effect on the conformational spaces of the lasso and branched-cyclic topoisomers (Fig. 2b). The lasso structures tend to expand with the metal ion adduction, as in the case of sphingonodin I, caulonodin III and microcin J25. However, this trend is not observed in the case of syanodin I where the $\overline{CCS}_{Metal}$ are smaller relative to the $\overline{CCS}_H$, suggesting a compacting behavior upon metalation (Fig. 2b). Moreover, $\overline{CCS}_{Metal}$ generally tend to increase with the ionic radius of the metal ion for the lasso peptides (Fig. 2b). This trend was clearly observed for the doubly alkali metalated species, for which the $\overline{CCS}_{2Cs} > \overline{CCS}_{2K} > \overline{CCS}_{2Na} > \overline{CCS}_{2H}$ induced an expanding of the lasso structures upon metalation. In addition, this trend was also observed in the case of syanodin I, for which the metalation results in a compacting behavior. However, this
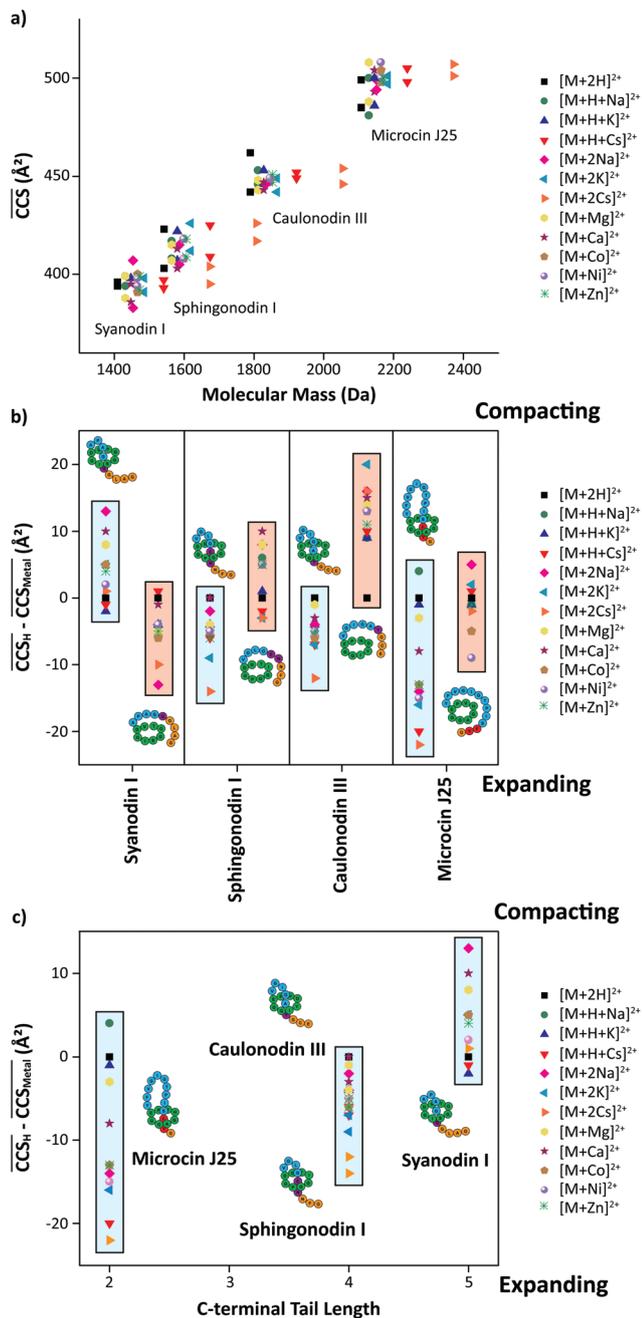
**Fig. 2** (a) $\overline{CCS}$ for all lasso and branched-cyclic peptides as a function of the molecular mass of the observed protonated (black), sodiated (dark green and magenta), potassiated (dark and light blue), cesiated (red and dark orange), magnesiated (yellow), calciated (purple), cobaltiated (brown), nickelated (light purple) and zincated (light green) species. (b) Effect of the metalated species on the lasso (blue) and branched-cyclic (red) conformational spaces. (c) Effect of the metalated species on the lasso conformational spaces as a function of the C-terminal length.

showed that the divalent metalated species generally favor the compacting or expanding behavior for lasso peptides as compared to the singly monovalent metalated species with similar ionic radius (Fig. 2b). These trends were clearly observed for syanodin I and microcin J25 where the divalent metal ions induced more compact and extended conformations, respectively. The same trends were also observed for the branched-cyclic peptides. The divalent metal ions interact with a higher number of ionic chemical bonds as compared to the singly monovalent metal ions with the same ionic radius.

Further inspection of the lasso structures reveals that these observations are related to the lengths of the loop and the C-terminal tail of the lasso peptides (Fig. 2c and S4b†). In fact, the steric stabilization of the C-terminal region inside of the macrolactam ring in lasso peptides allows only for distinct interactions of the metal ion with either residues in the loop or tail region. This limits the size of the interacting region and apparently leads to a bias of metal ion binding in either the loop or tail region, depending whichever section is larger in the respective lasso peptide. For example, the short loop (4 residues) and the long C-terminal tail (5 residues) of syanodin I suggest that the metal ions are interacting with the C-terminal tail, inducing a compacting of the flexible C-terminal tail (Fig. 2c and S4b†). Conversely, for microcin J25, the larger loop (11 residues) and the shorter C-terminal tail (2 residues) indicate that the metal ions are probably interacting with the loop, implying an expansion of this region (Fig. 2c and S4b†). For the unthreaded branched-cyclic peptides, incorporating a metal ion induces different type of structures by interacting in a different way with the metal ions. In fact, the branched-cyclic form of syanodin I and microcin J25 tended to expand with the metal ion adduction, while sphingonodin I and caulonodin III adopted a more compact structure. The latter behavior probably arises from the non-restricted flexible C-terminal tail that can form additional intramolecular binding interactions with the metal ions. In fact, the non-restricted C-terminal tail of the branched-cyclic topology allows metal coordination by residues throughout this region, which can result in gas-phase structures that are sometimes even more compact than the lasso peptides, for which the topology may be preserved or stabilized upon metal ion binding limiting their conformational changes.

Previous reports hypothesized that lasso peptides produced by gene clusters in proximity of a lasso peptide isopeptidase encoding gene might act like metallophores.[92,93] That is, that they would act as scavenger molecules for certain metal ions, which would in turn be released upon lasso peptide isopeptidase-mediated degradation inside the cells. If this hypothesis would hold true for the tested lasso peptide caulonodin III, sphingonodin I and syanodin I (microcin J25 is not produced by gene clusters with a lasso peptide isopeptidase encoding gene), a single distinct conformation would appear in the IMS distribution due to the specific interactions typical for metallophore-metal ion complexes. This was not observed with any of the tested metal ions including the typical metallophore targets as copper and iron metal ions, except for the single

trend was not observed for all the branched-cyclic structures, involving that these peptides can fully interact with metal ions thanks to their completely flexible C-terminal part resulting in distinct rearrangements (Fig. 2b). The nature of the metal ions

alkali (Na, K and Cs) species of caulonodin III and the nicke-lated species of syanodin I (Fig. 1, S3 and S5†). In fact, multiple IMS bands with distinct CCS were observed in all these cases suggesting multiple interactions of the metal ions with the lasso peptides under these conditions.

### Influence of metal ions on lasso and branched-cyclic topoisomer analytical screening

Although lasso peptides and their corresponding branched-cyclic topoisomers share the same amino acid sequence, they can be differentiated based on their secondary structures.[94] In a previous work, we showed the potential of native nESI-TIMS-MS as a high throughput screening tool for identification of lasso and branched-cyclic topologies.[87] Briefly, TIMS-MS using fast scan rates resulted in baseline separation for doubly protonated species of sphingonodin I ($r$ = 2.8, Fig. S6a†), caulonodin III ($r$ = 2.5, Fig. S7a†) and microcin J25 ($r$ = 1.9, Fig. S8a†).[87] However, only partial separation was observed for syanodin I topoisomers ($r$ = 0.7, Fig. 3a) using fast scan rates. A known alternative to increase the analytical power of IMS techniques is the use of metalation.[44–47] In fact, metalated species tend to differ in conformation from their protonated analogs as the metal ions may bind to different sites and/or coordinate differently because of their chemical differences, potentially leading to effective IMS separation.[43]

The effect of alkali (Na, K and Cs), alkaline earth (Mg and Ca) and transition (Co, Ni and Zn) metal ions on the TIMS separation of lasso and branched-cyclic topoisomers is illustrated in Fig. 3, S6, S7 and S8† for syanodin I, sphingonodin I, caulonodin III and microcin J25, respectively. Inspection of Fig. 3 shows that for all cases, except the singly sodiated ($r$ = 0.2, Fig. 3b) and potassiated ($r$ = 0.5, Fig. 3c) species, the metalated species resulted in higher IMS resolution ($r$, by at least a factor of 2) between the lasso and branched-cyclic topoisomers compared to the IMS resolution achieved using the protonated species, enabling their identification at fast scan rates (Table S2†). Concerning sphingonodin I (Fig. S6 and Table S3†), caulonodin III (Fig. S7 and Table S4†) and microcin J25 (Fig. S8 and Table S5†), for which protonated species are well resolved, the metalated species generally did not improve or resulted in comparable IMS resolution as compared to the protonated species. However, several metal ions allowed to obtain higher IMS resolution in the case of the singly potassiated ($r$ = 4.7, Fig. S6c†) and cesiated ($r$ = 4.8, Fig. S6d†) species for sphingonodin I, the magnesiated ($r$ = 3.3, Fig. S7h†) species for caulonodin III and the magnesiated ($r$ = 2.6, Fig. S8h†), calciated ($r$ = 3.8, Fig. S8i†), cobaltiated ($r$ = 3.2, Fig. S8j†), nickelated ($r$ = 3.4, Fig. S8k†) and zincated ($r$ = 3.4, Fig. S8l†) species for microcin J25. The most pronounced difference was observed for the $[M + 2Na]^{2+}$ ($r$ = 3.4, Fig. 3e), $[M + H + Cs]^{2+}$ ($r$ = 4.8, Fig. S6d†), $[M + Mg]^{2+}$ ($r$ = 3.3, Fig. S7h†) and $[M + Ca]^{2+}$ ($r$ = 3.8, Fig. S8i†) species of syanodin I, sphingonodin I, caulonodin III and microcin J25, respectively.

All these results did not display a general trend in term of IMS resolution and therefore suggest that metal ion binding
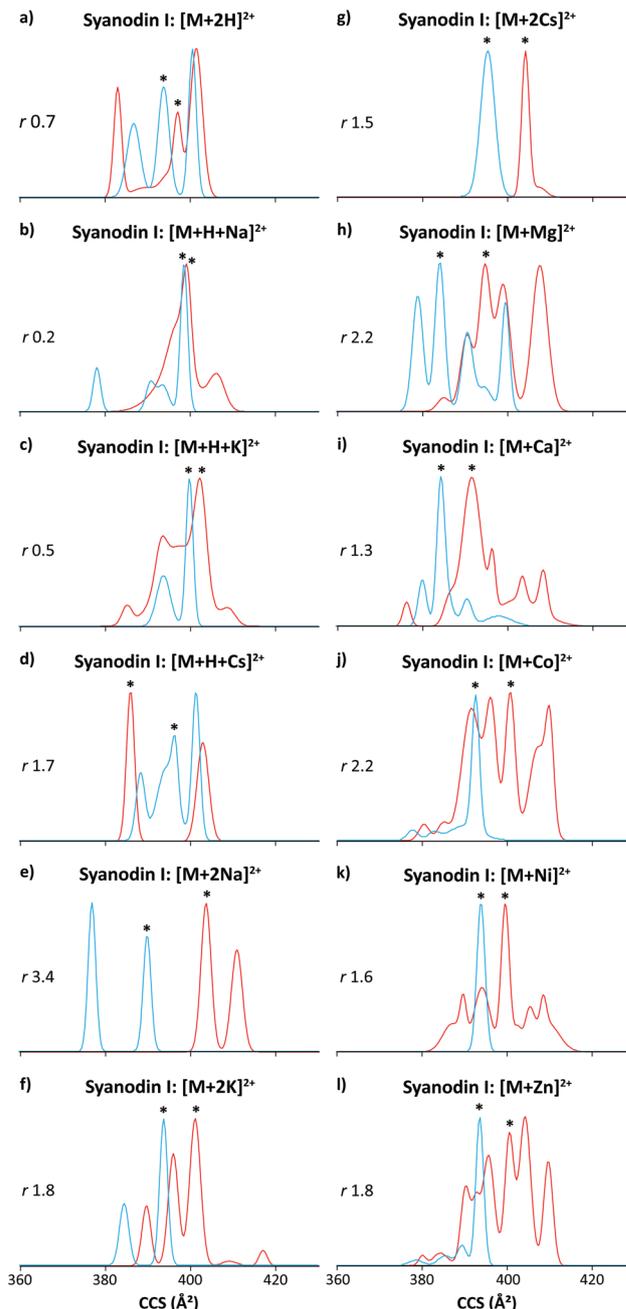


**Fig. 3** Typical TIMS spectra for syanodin I (blue traces) and its branched-cyclic topoisomer (red traces) in the (a) protonated, (b, e) sodiated, (c, f) potassiated, (d, g) cesiated, (h) magnesiated, (i) calciated, (j) cobaltiated, (k) nickelated and (l) zincated form. A typical Sr of 0.56 V m$^{-1}$ s$^{-1}$ was used and the resolution ($r$) values are given. The peaks highlighted by * symbols were taken to calculate the resolution.

rearrange lasso and branched-cyclic structures in different ways, which involves trying diverse metal ions to maximize resolution. However, a different number of IMS bands are observed as a function of the metal ion size for the same charge state in both topoisomers. For example, while the TIMS distribution of the metalated lasso and branched-cyclic peptide ions typically consisted of multiple bands, the TIMS

distribution of the doubly cesiated species resulted in a single band for each lasso and branched-cyclic peptide couple (except for microcin J25 branched-cyclic that presents two minor IMS bands), therefore improving the discrimination between these topoisomers in the gas-phase (Fig. 3g, S6g, S7g and S8g†). The presence of the two additional minor IMS bands for the branched-cyclic form of microcin J25 (Fig. S8g†) could be explained by the longer length of its C-terminal region (13 residues, Table 1), as compared to the other branched-cyclic peptides (9 residues, Table 1), which significantly increase the flexibility of this region, permitting additional interactions with the cesium ions. These results illustrate the potential of the doubly cesiated species to provide a unique conformation as an efficient analytical feature for the identification of the lasso fold and corresponding branched-cyclic topoisomers at physiological conditions, using high resolution native nESI-TIMS.

The high mobility resolving power of TIMS resulted in the separation of metalated lasso and branched-cyclic peptide ions ($r \sim 2.1$ on average). The added analytical advantages of metalation to the nESI-TIMS-MS were particularly illustrated in the case of syanodin I topoisomers, where the differences in the IMS profiles are significantly increased with metalation. Conversely, for the well resolved sphingonodin I, caulonodin III and microcin J25, the metalation generally did not improve separation and resulted in comparable IMS resolution as found for the protonated species. Results showed that the metal ion binding can rearrange lasso and branched-cyclic structures in distinct ways. Moreover, metalation (e.g., using the doubly cesiated species) can result in simplification of the mobility profiles down to a single conformation and thus can be utilized as a way to maximize the analytical power of high resolution TIMS for the discrimination of lasso and branched-cyclic topologies at physiological conditions.

## Conclusions

The potential of native nESI-TIMS-MS as a powerful tool for the investigation of the conformational changes upon alkali (Na, K and Cs), alkaline earth (Mg and Ca) and transition (Co, Ni and Zn) metalation of four lasso peptides (syanodin I, sphingonodin I, caulonodin III and microcin J25) and their branched-cyclic topoisomers was studied. The present results showed that the nature of the metal ions plays a significant role in the conformational motifs, as reflected by the substantial changes in the IMS distributions as compared to the protonated species. In addition, the high mobility resolving power of TIMS permitted to group conformational families that are preserved regardless of which metal ion is incorporated. The lower diversity of conformational families for syanodin I as compared to the other lasso peptides supported syanodin I probably forms tighter binding interactions with metal ions limiting their conformational changes in the gas-phase. Conversely, the higher diversity of conformational families for the branched-cyclic topologies further supported that the metal ions probably interact with a higher number of electronegative groups arising from the fully unconstraint C-terminal part.

A correlation between the lengths of the loop and the C-terminal tail with the conformational spaces of the lasso peptides becomes apparent upon addition of metal ions. The steric stabilization of the C-terminal region inside of the macrolactam ring in lasso peptides allows only for distinct interactions of the metal ion with either residues in the loop or tail region. This limits the size of the interacting region and apparently leads to a bias of metal ion binding in either the loop or tail region, depending whichever section is larger in the respective lasso peptide. For branched-cyclic peptides, the non-restricted C-terminal tail allows metal coordination by residues throughout this region, which can result in gas-phase structures that are sometimes even more compact than the lasso peptides.

## Author contributions

The manuscript was written through contributions of all authors. All authors have given approval to the final version of the manuscript.

## Conflicts of interest

The authors declare no competing financial interest.

## Acknowledgements

## References

1 H. Siegel and A. Siegel, *Biological Action of Metal Ions*, Marcel Dekker, New York, 1976.
2 C. M. Gomes and P. Wittung-Stafshede, *Protein Folding and Metal Ions: Mechanisms, Biology and Disease*, Taylor & Francis, Boca Raton, 2011.
3 E. A. Permyakov, *Metalloproteomics*, Wiley, New Jersey, 2009.
4 B. Zambelli, F. Musiani and S. Ciurli, *Met. Ions Life Sci.*, 2012, **10**, 135–170.
5 L. M. Teesch, R. C. Orlando and J. Adams, *J. Am. Chem. Soc.*, 1991, **113**, 3668–3675.
6 J. A. Loo, P. Hu and R. D. Smith, *J. Am. Soc. Mass Spectrom.*, 1994, **5**, 959–965.

7  O. V. Nemirovskiy and M. L. Gross, *J. Am. Soc. Mass Spectrom.*, 1998, **9**, 1020–1028.

8  P. F. Hu and J. A. Loo, *J. Am. Chem. Soc.*, 1995, **117**, 11314–11319.

9  P. B. Armentrout, M. T. Rodgers, J. Oomens and J. D. Steill, *J. Phys. Chem. A*, 2008, **112**, 2248–2257.

10  T. Wyttenbach, D. Liu and M. T. Bowers, *J. Am. Chem. Soc.*, 2008, **130**, 5993–6000.

11  R. H. Holm, P. Kennepohl and E. I. Solomon, *Chem. Rev.*, 1996, **96**, 2239–2314.

12  M. J. Page and E. Di Cera, *Physiol. Rev.*, 2006, **86**, 1049–1092.

13  C. Zentz, G. Chottard and J. Bolard, *J. Inorg. Nucl. Chem.*, 1978, **40**, 2019–2023.

14  L. Quintanar and L. Rivillas-Acevedo, *Methods Mol. Biol.*, 2013, **1008**, 267–297.

15  I. Bertini, P. Turano and A. J. Vila, *Chem. Rev.*, 1993, **93**, 2833–2932.

16  M. R. Jensen, M. A. Hass, D. F. Hansen and J. J. Led, *Cell. Mol. Life Sci.*, 2007, **64**, 1085–1104.

17  E. Ennifar, P. Walter and P. Dumas, *Nucleic Acids Res.*, 2003, **31**, 2671–2682.

18  S. E. J. Bowman, J. Bridwell-Rabb and C. L. Drennan, *Acc. Chem. Res.*, 2016, **49**, 695–702.

19  M. Kohtani, B. S. Kinnear and M. F. Jarrold, *J. Am. Chem. Soc.*, 2000, **122**, 12377–12378.

20  M. K. Drayss, P. B. Armentrout, J. Oomens and M. Schaefer, *Int. J. Mass Spectrom.*, 2010, **297**, 18–27.

21  J. Pan and L. Konermann, *Biochemistry*, 2010, **49**, 3477–3486.

22  L. Deng, N. Sun, E. N. Kitova and J. S. Klassen, *Anal. Chem.*, 2010, **82**, 2170–2174.

23  J. T. Hopper and N. J. Oldham, *Anal. Chem.*, 2011, **83**, 7472–7479.

24  J. B. Fenn, M. Mann, C. K. Meng, S. F. Wong and C. M. Whitehouse, *Science*, 1989, **246**, 64–71.

25  L. M. Teesch and J. Adams, *J. Am. Chem. Soc.*, 1991, **113**, 812–820.

26  H. M. Watson, J. B. Vincent and C. J. Cassady, *J. Mass Spectrom.*, 2011, **46**, 1099–1107.

27  H. Liu and K. Hakansson, *Anal. Chem.*, 2006, **78**, 7570–7576.

28  A. J. Kleinnijenhuis, R. Mihalca, R. M. A. Heeren and A. J. R. Heck, *Int. J. Mass Spectrom.*, 2006, **253**, 217–224.

29  W. A. Tao, D. Zhang, E. N. Nikolaev and R. G. Cooks, *J. Am. Chem. Soc.*, 2000, **122**, 10598–10609.

30  J. Zhang and J. S. Brodbelt, *J. Mass Spectrom.*, 2003, **38**, 555–572.

31  J. Zhang and J. S. Brodbelt, *Anal. Chem.*, 2005, **77**, 1761–1770.

32  Y. Wu, C. Guo, N. Zhang, G. Bian and K. Jiang, *Rapid Commun. Mass Spectrom.*, 2014, **28**, 2111–2120.

33  L. Han and C. E. Costello, *J. Am. Soc. Mass Spectrom.*, 2011, **22**, 997–1013.

34  D. E. Clemmer, R. R. Hudgins and M. F. Jarrold, *J. Am. Chem. Soc.*, 1995, **117**, 10141–10142.

35  F. Lanucara, S. W. Holman, C. J. Gray and C. E. Eyers, *Nat. Chem.*, 2014, **6**, 281–294.

36  D. R. Fuller, M. S. Glover, N. A. Pierson, D. Kim, D. H. Russell and D. E. Clemmer, *J. Am. Soc. Mass Spectrom.*, 2016, **27**, 1376–1382.

37  C. Wu, J. Klasmeier and H. H. Hill, *Rapid Commun. Mass Spectrom.*, 1999, **13**, 1138–1142.

38  Y. Berezovskaya, C. T. Armstrong, A. L. Boyle, M. Porrini, D. N. Woolfson and P. E. Barran, *Chem. Commun.*, 2011, **47**, 412–414.

39  M. Kohtani, M. F. Jarrold, S. Wee and R. A. J. O'Hair, *J. Phys. Chem. B*, 2004, **108**, 6093–6097.

40  T. Wyttenbach, M. Witt and M. T. Bowers, *J. Am. Chem. Soc.*, 2000, **122**, 3458–3464.

41  Y. Seo, M. R. Schenauer and J. A. Leary, *Int. J. Mass Spectrom.*, 2011, **303**, 191–198.

42  V. E. Wright, F. Castro-Gómez, E. Jurneczko, J. C. Reynolds, A. Poulton, S. D. R. Christie, P. Barran, C. Bo and C. S. Creaser, *Int. J. Ion Mobil. Spectrom.*, 2013, **16**, 61–67.

43  J. M. Dilger, S. J. Valentine, M. S. Glover, M. A. Ewing and D. E. Clemmer, *Int. J. Mass Spectrom.*, 2012, **330**, 35–45.

44  T. G. Flick, I. D. Campuzano and M. D. Bartberger, *Anal. Chem.*, 2015, **87**, 3300–3307.

45  V. Domalain, V. Tognetti, M. Hubert-Roux, C. M. Lange, L. Joubert, J. Baudoux, J. Rouden and C. Afonso, *J. Am. Soc. Mass Spectrom.*, 2013, **24**, 1437–1445.

46  B. H. Clowers and H. H. Hill Jr., *J. Mass Spectrom.*, 2006, **41**, 339–351.

47  M. D. Leavell, S. P. Gaucher, J. A. Leary, J. A. Taraszka and D. E. Clemmer, *J. Am. Soc. Mass Spectrom.*, 2002, **13**, 284–293.

48  F. A. Fernandez-Lima, D. A. Kaplan, J. Suetering and M. A. Park, *Int. J. Ion Mobility Spectrom.*, 2011, **14**, 93–98.

49  F. A. Fernandez-Lima, D. A. Kaplan and M. A. Park, *Rev. Sci. Instrum.*, 2011, **82**, 126106.

50  D. R. Hernandez, J. D. Debord, M. E. Ridgeway, D. A. Kaplan, M. A. Park and F. Fernandez-Lima, *Analyst*, 2014, **139**, 1913–1921.

51  P. Benigni, C. J. Thompson, M. E. Ridgeway, M. A. Park and F. Fernandez-Lima, *Anal. Chem.*, 2015, **87**, 4321–4325.

52  P. Benigni and F. Fernandez-Lima, *Anal. Chem.*, 2016, **88**, 7404–7412.

53  P. Benigni, K. Sandoval, C. J. Thompson, M. E. Ridgeway, M. A. Park, P. Gardinali and F. Fernandez-Lima, *Environ. Sci. Technol.*, 2017, **51**, 5978–5988.

54  K. J. Adams, D. Montero, D. Aga and F. Fernandez-Lima, *Int. J. Ion Mobility Spectrom.*, 2016, **19**, 69–76.

55  A. Castellanos, P. Benigni, D. R. Hernandez, J. D. DeBord, M. E. Ridgeway, M. A. Park and F. A. Fernandez-Lima, *Anal. Methods*, 2014, **6**, 9328–9332.

56  E. R. Schenk, V. Mendez, J. T. Landrum, M. E. Ridgeway, M. A. Park and F. Fernandez-Lima, *Anal. Chem.*, 2014, **86**, 2019–2024.

57  J. C. Molano-Arevalo, D. R. Hernandez, W. G. Gonzalez, J. Miksovska, M. E. Ridgeway, M. A. Park and F. Fernandez-Lima, *Anal. Chem.*, 2014, **86**, 10223–10230.

58  A. McKenzie-Coe, J. D. DeBord, M. Ridgeway, M. Park, G. Eiceman and F. Fernandez-Lima, *Analyst*, 2015, **140**, 5692–5699.

59  A. Garabedian, D. Butcher, J. L. Lippens, J. Miksovska, P. P. Chapagain, D. Fabris, M. E. Ridgeway, M. A. Park and F. Fernandez-Lima, *Phys. Chem. Chem. Phys.*, 2016, **18**, 26691–26702.

60  M. E. Ridgeway, J. A. Silveira, J. E. Meier and M. A. Park, *Analyst*, 2015, **140**, 6964–6972.

61  F. Meier, S. Beck, N. Grassl, M. Lubeck, M. A. Park, O. Raether and M. Mann, *J. Proteome Res.*, 2015, **14**, 5378–5387.

62  J. A. Silveira, M. E. Ridgeway and M. A. Park, *Anal. Chem.*, 2014, **86**, 5624–5627.

63  Y. Pu, M. E. Ridgeway, R. S. Glaskin, M. A. Park, C. E. Costello and C. Lin, *Anal. Chem.*, 2016, **88**, 3440–3443.

64  F. C. Liu, S. R. Kirk and C. Bleiholder, *Analyst*, 2016, **141**, 3722–3730.

65  A. Garabedian, P. Benigni, C. E. Ramirez, *et al.*, *J. Am. Soc. Mass Spectrom.*, 2017, DOI: 10.1007/s13361-017-1787-8.

66  E. R. Schenk, M. E. Ridgeway, M. A. Park, F. Leng and F. Fernandez-Lima, *Anal. Chem.*, 2014, **86**, 1210–1214.

67  K. Jeanne Dit Fouque, A. Garabedian, J. Porter, M. Baird, X. Pang, T. D. Williams, L. Li, A. Shvartsburg and F. Fernandez-Lima, *Anal. Chem.*, 2017, **89**, 11787–11794.

68  E. R. Schenk, R. Almeida, J. Miksovska, M. E. Ridgeway, M. A. Park and F. Fernandez-Lima, *J. Am. Soc. Mass Spectrom.*, 2015, **26**, 555–563.

69  J. C. Molano-Arevalo, K. Jeanne Dit Fouque, K. Pham, J. Miksovska, M. E. Ridgeway, M. A. Park and F. Fernandez-Lima, *Anal. Chem.*, 2017, **89**, 8757–8765.

70  P. Benigni, R. Marin, J. C. Molano-Arevalo, A. Garabedian, J. J. Wolff, M. E. Ridgeway, M. A. Park and F. Fernandez-Lima, *Int. J. Ion Mobility Spectrom.*, 2016, **19**, 95–104.

71  J. D. Hegemann, M. Zimmermann, X. Xie and M. A. Marahiel, *Acc. Chem. Res.*, 2015, **48**, 1909–1919.

72  M. O. Maksimov, S. J. Pan and A. James Link, *Nat. Prod. Rep.*, 2012, **29**, 996–1006.

73  J. D. Hegemann, M. Zimmermann, S. Zhu, D. Klug and M. A. Marahiel, *Biopolymers*, 2013, **100**, 527–542.

74  J. D. Hegemann, M. Zimmermann, X. Xie and M. A. Marahiel, *J. Am. Chem. Soc.*, 2013, **135**, 210–222.

75  M. O. Maksimov and A. J. Link, *J. Ind. Microbiol. Biotechnol.*, 2014, **41**, 333–344.

76  M. O. Maksimov, I. Pelczer and A. J. Link, *Proc. Natl. Acad. Sci. U. S. A.*, 2012, **109**, 15223–15228.

77  R. D. Kersten, Y. L. Yang, Y. Xu, P. Cimermancic, S. J. Nam, W. Fenical, M. A. Fischbach, B. S. Moore and P. C. Dorrestein, *Nat. Chem. Biol.*, 2011, **7**, 794–802.

78  J. I. Tietz, C. J. Schwalen, P. S. Patel, T. Maxson, P. M. Blair, H. C. Tai, U. I. Zakai and D. A. Mitchell, *Nat. Chem. Biol.*, 2017, **13**, 470–478.

79  T. A. Knappe, F. Manzenrieder, C. Mas-Moruno, U. Linne, F. Sasse, H. Kessler, X. Xie and M. A. Marahiel, *Angew. Chem., Int. Ed.*, 2011, **50**, 8714–8717.

80  J. D. Hegemann, M. De Simone, M. Zimmermann, T. A. Knappe, X. Xie, F. S. Di Leva, L. Marinelli, E. Novellino, S. Zahler, H. Kessler and M. A. Marahiel, *J. Med. Chem.*, 2014, **57**, 5829–5834.

81  J. D. Hegemann, C. D. Fage, S. Zhu, K. Harms, F. S. Di Leva, E. Novellino, L. Marinelli and M. A. Marahiel, *Mol. Biosyst.*, 2016, **12**, 1106–1109.

82  M. Zimmermann, J. D. Hegemann, X. Xie and M. A. Marahiel, *Chem. Biol.*, 2013, **20**, 558–569.

83  T. A. Knappe, U. Linne, L. Robbel and M. A. Marahiel, *Chem. Biol.*, 2009, **16**, 1290–1298.

84  R. A. Salomon and R. N. Farias, *J. Bacteriol.*, 1992, **174**, 7428–7435.

85  J. O. Solbiati, M. Ciaccio, R. N. Farias, J. E. Gonzalez-Pastor, F. Moreno and R. A. Salomon, *J. Bacteriol.*, 1999, **181**, 2659–2662.

86  E. W. McDaniel and E. A. Mason, *Mobility and diffusion of ions in gases*, John Wiley and Sons, Inc., New York, New York, 1973.

87  K. Jeanne Dit Fouque, J. Moreno, J. D. Hegemann, S. Zirah, S. Rebuffat and F. Fernandez-Lima, *Anal. Chem.*, 2018, **90**, 5139–5146.

88  K. Jeanne Dit Fouque, H. Lavanant, S. Zirah, J. Lemoine, S. Rebuffat, J. C. Tabet, A. Kulesza, C. Afonso, P. Dugourd and F. Chirot, *Rapid Commun. Mass Spectrom.*, 2015, **29**, 1411–1419.

89  K. Jeanne Dit Fouque, H. Lavanant, S. Zirah, V. Steinmetz, S. Rebuffat, P. Maitre and C. Afonso, *J. Phys. Chem. A*, 2016, **120**, 3810–3816.

90  K. J. Rosengren, R. J. Clark, N. L. Daly, U. Goeransson, A. Jones and D. J. Craik, *J. Am. Chem. Soc.*, 2003, **125**, 12464–12474.

91  J. A. Taraszka, A. E. Counterman and D. E. Clemmer, *Int. J. Mass Spectrom.*, 2001, **204**, 87–100.

92  M. O. Maksimov and A. J. Link, *J. Am. Chem. Soc.*, 2013, **135**, 12038–12047.

93  J. R. Chekan, J. D. Koos, C. Zong, M. O. Maksimov, A. J. Link and S. K. Nair, *J. Am. Chem. Soc.*, 2016, **138**, 16452–16458.

94  K. Jeanne Dit Fouque, C. Afonso, S. Zirah, J. D. Hegemann, M. Zimmermann, M. A. Marahiel, S. Rebuffat and H. Lavanant, *Anal. Chem.*, 2015, **87**, 1166–1172.